Dalton Transactions

ROYAL SOCIETY OF CHEMISTRY

PAPER

View Article Online
View Journal | View Issue

Cite this: *Dalton Trans.*, 2023, **52**, 962

Influence of alkali metal cations on the formation of the heterobimetallic actinide *tert*-butoxides $[AnM_3(O^tBu)_7]$ and $[AnM_2(O^tBu)_6]$ (An^{IV} = Th, U; M^I = Li, Na, K, Rb, Cs)†

Andreas Lichtenberg, [a] Markus Zegke, [a] Gary S. Nichol, [b] Aida Raauf *[a] and Sanjay Mathur *[a]

Received 27th April 2022,
Accepted 16th December 2022

DOI: 10.1039/d2dt01316a

rsc.li/dalton

Heterobimetallic *tert*-butoxides of alkali metal cations with tetravalent actinide centers exhibit two distinctive structural motifs, $[AnM_2(O^tBu)_6]$ and $[AnM_3(O^tBu)_7]$ (An^{IV} = Th, U and M^I = Li, Na, K, Rb, Cs), evidently governed by the size of the alkali metal ions. Both $[AnM_3(O^tBu)_7]$ **AnM3** (An^{IV} = U, M^I = Li; An^{IV} = Th, M^I = Li, Na) and $[AnM_2(O^tBu)_6]$ **AnM2** (An^{IV} = U, M^I = Na–Cs; An^{IV} = Th, M^I = K–Cs) compounds are obtained in nearly quantitative yields by reacting actinide and alkali metal silyl amides with an excess of *tert*-butyl alcohol. The **AnM3** complexes form a cubane-type coordination motif, whereas the **AnM2** complexes display a geometry resembling two face-shared bipyramids. The sodium derivatives of thorium and uranium (**ThNa3** and **UNa2**) allow the determination of the structural transition threshold as a function of the ratio of the ionic radii $r_i(An^{IV})/r_i(M^I)$. The **AnM3** complexes are formed for ratios above 0.92 and the **AnM2** type is formed for ratios below 0.87. All compounds are unambiguously characterized in both solution and solid states by NMR and IR spectroscopic studies and single crystal X-ray diffraction analyses, respectively.

Introduction

Metal alkoxides[1] have found a broad range of applications, for instance in catalysis[2–4] and material synthesis.[5–11] There is relatively little information on actinide alkoxides, and the published data on uranium alkoxides relate to the original contributions of Henry Gilman and Don Bradley, which were instrumental in the design of this study. In addition to new synthetic routes, this work focuses on the solid-state structural chemistry of actinide alkoxides and the flexibility of their coordination sphere to accommodate different ligands and co-ligands as well as their propensity to coordinate to other metal alkoxides to form heterobimetallic frameworks.[12–23] The latter, due to renewed interest in various generation IV nuclear reactor concepts, where new real and simulated fuels will be prepared for studies of properties required for certification, could be prepared by alkoxide based sol–gel processing.[24–27] In this context, the preparation of heterometallic actinide alkoxides containing metals, found as fission products in nuclear reactors (*e.g.* cesium), is of interest.

The influence of the ionic size upon the formation of novel heterometallic actinide complexes provides new opportunities for the design and synthesis of new compounds and shows the effect upon the precise constituents, including the basic octahedral coordination environment of the actinide alkoxide. Besides the investigation of the molecular structure and the coordination chemistry of the actinides, the examination of the systematic variation of the ion size provides a fundamental understanding of the functional and specific properties of novel actinide materials.[28–31] For instance, a recently reported study shows that the hydration enthalpy of heterometallic actinide compounds correlates with the ionic size of the heterocation.[32]

An informative overview of the formation of hetero (bi- and tri) metallic alkoxide derivatives was provided in the review of Veith and Mathur *et al.* including several alkoxide structure-types upon various valences of the metal centres.[33] The review of Sattelberger *et al.* additionally provides an insight into the field of actinide alkoxide chemistry.[22] However, the authors warn the reader that some of the early works on actinide alkoxides referenced in the review may not be totally reliable.

[a]*Institute of Inorganic Chemistry, University of Cologne, 50939 Cologne, Germany. E-mail: aida.raauf@uni-koeln.de, sanjay.mathur@uni-koeln.de*
[b]*School of Chemistry, The University of Edinburgh, David Brewster Road EH9 3FJ, Edinburgh, Scotland, UK*

†Electronic supplementary information (ESI) available. CCDC 2152017–2152026. For ESI and crystallographic data in CIF or other electronic format see DOI: https://doi.org/10.1039/d2dt01316a

Nevertheless, some more valid structures have been published afterwards.

Monovalent alkali metal alkoxides of thorium and uranium with a trinuclear framework have been reported, such as $[U_2K(O^tBu)_9]$[34] (**U2K**) or $[Th_2Na(O^tBu)_9]$[35] (**Th2Na**) and $[ULi_2(O^tBu)_6(THF)_2]$[23] (**ULi2-THF**). The heterobimetallic An^{IV}–M^I compounds (An = Th, M = Na; An = U, M = Li, K) were obtained either through a salt metathesis reaction of UCl_4 and 6 eq. of $Li(O^tBu)$ in THF[23] or by Lewis acid–base interactions among $[An_2(O^tBu)_8(HO^tBu)]$ (An = Th, U) and $M(O^tBu)$ (M = Na, K).[21,35] Attempts to increase (>2) the alkali metal : actinide stoichiometry to obtain the tetranuclear species **AnM3** have been made; however, such compounds could not be isolated and structurally investigated.[23]

The influence of the ionic size of the metal cations is a key feature of the structural chemistry of metal alkoxides with a series of alkali metal *tert*-butoxides $[M^I(O^tBu)]_n$ delivering a prominent example.[11,36,37] Lithium *tert*-butoxide (M^I = Li) for instance is found to be octameric (n = 8),[38] however the larger sodium forms a hexameric (n = 6) framework.[39] The nuclearity is found to decrease for larger cations (K, Rb, Cs) with potassium, rubidium or cesium *tert*-butoxides crystallizing in a tetrameric cubane-type structure (n = 4).[36] Other examples are our recently reported iron-lanthanide alkoxides, where the size of the Ln^{3+} cations was found to affect the Ln : Fe ratio in the molecular structure.[11] Such structural transformations are mainly affected by the ionic radii of the constituting metals and the steric requirement of the applied alkoxide ligands.

In this work, we have investigated the structural diversity in a series of alkali metal actinide alkoxides based on the complexation of *tert*-butoxides of alkali metal cations and tetravalent uranium and thorium. The heterobimetallic actinide-alkali metal alkoxides have been obtained by a ligand exchange reaction starting from the An^{IV} metallacycle compound $[AnN'N''_2]$ (An^{IV} = Th, U, N′ = {$(CH_2SiMe_2)N(SiMe_3)$}, N″ = {$N(SiMe_3)_2$}) and monovalent alkali metal silylamides with *tert*-butyl-alcohol in a nonpolar hydrocarbon solvent.

Results and discussion

Synthesis of the An^{IV}–M^I *tert*-butoxide compounds

The An^{IV}–M^I *tert*-butoxides of the general formula $[AnM_3(O^tBu)_7]$ (**AnM3**-type: **ULi3** (CCDC: 2152019), **ThLi3** (CCDC: 2152017), **ThNa3** (CCDC: 2152018)) and $[AnM_2(O^tBu)_6]$ (**AnM2**-type: **UNa2** (CCDC: 2152025), **UK2** (CCDC: 2152024), **ThK2** (CCDC: 2152021), **URb2** (CCDC: 2152026), **ThRb2** (CCDC: 2152022), **UCs2** (CCDC: 2152023), **ThCs2** (CCDC: 2152020))† were synthesized through a reaction of 1 eq. of $[AnN'N''_2]$ (An^{IV} = Th, U) and 2 or 3 eq. of [MN″] (M^I = Li, Na, K, Rb, Cs) with 6 or 7 eq. of HO^tBu (Scheme 1).

The targeted formation of the **AnM3** and **AnM2** structures was controlled by the ratio of the ionic radii of the An^{IV} and M^I centers. For instance, the smallest of the alkali metal cations, lithium (0.76 Å), yielded the **AnM3** structural types for both uranium (0.89 Å) and thorium (0.94 Å), whereas the formation of **AnM2** compounds was favored with increasing ionic radii of potassium (1.38 Å), rubidium (1.52 Å) and cesium (1.67 Å). The sodium (1.02 Å) derivatives represent a borderline case with both structure types **ThNa3** and **UNa2** observed as thermodynamically favored arrangements of cations.[40]

Calculating the ratio of the ionic radii $r_i(An^{IV})/r_i(M^I)$ (for C. N. 6) allowed us to define the threshold of the structural transition in the M(I)–An(IV) series of mixed-metal *tert*-butoxides. The **AnM3** structures were typically obtained for a $r_i(An^{IV})/r_i(M^I)$ ratio of 0.92 or higher. Herein, three smaller alkali metals can bind towards the *tert*-butoxide octahedron surrounding the An^{IV} center. The **AnM2** structure is formed below a ratio of 0.87 that reasonably explains the increased space requirement for the larger alkali metal cations. The transition threshold for both structures is apparently located between

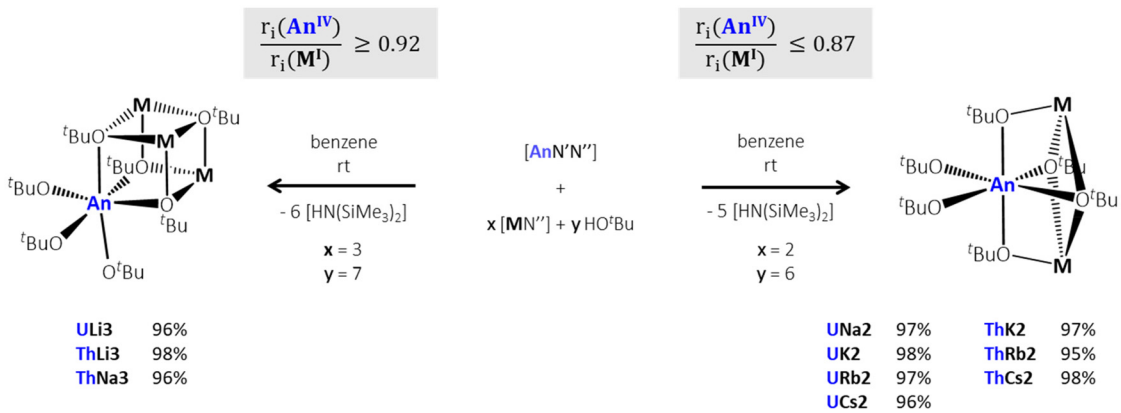

Scheme 1 Synthesis of $[AnM_3(O^tBu)_7]$ **AnM3** and $[AnM_2(O^tBu)_6]$ **AnM2** (An^{IV}: Th, U; M^I: Li, Na, K, Rb, Cs) by reacting [AnN′N″] with the stoichiometric ratio of [MN″] and HO^tBu in benzene at room temperature. The formation of different structural types simply depends on the ionic radius (r_i) ratio of An^{IV} to M^I.

a ratio of 0.87 and 0.92, which corroborates the formation of **UNa2** and **ThNa3**, respectively.

$[AnM_3(O^tBu)_7]$ derivatives (AnM3)

The molecular structures of **ThLi3**, **ULi3** and **ThNa3** display the An^{IV} center to be in a distorted octahedral coordination environment formed by six *tert*-butoxide groups out of which three bind terminally to the An^{IV} center, while the remaining three take a triply bridging position (μ_3-fashion) interconnecting the An^{IV} center to two of the M^I cations (Fig. 1). The seventh *tert*-butoxide ligand coordinates only to the three M^I centers in a μ_3-capping mode. The structure exhibits a distorted cubane-type $[AnM_3O_4]$ framework, with the four metal centers and four μ_3-bridged alkoxide ligands occupying the corners of a cube that is distorted due to discrepancy in the ionic size of Li^I (0.76 Å) and Th^{IV}/U^{IV} (0.94/0.89 Å).

Selected bond lengths, angles and metal–metal distances for **ULi3**, **ThLi3** and **ThNa3** are comparable to the previously reported *tert*-butoxides $[ULi_2(O^tBu)_6(THF)_2]$[23] **ULi2-THF**, $[U_2Li(O^tBu)_9(THF)]$[23] **U2Li-THF** and $[Th_2Na(O^tBu)_9]$[35] **Th2Na** as listed in Table S3.† The An^{IV}–O_t and An^{IV}–O_{μ_3} bond lengths are in good agreement with the literature reports for An^{IV} (Th, U) *tert*-butoxides. The An–M distances in the **AnM3** complexes were found to be increased (*ca.* 0.3 Å) when compared to the reported tetravalent actinide (Th, U) alkali metal *tert*-butoxides. This elongation can be attributed to the presence of the cubane-type geometry and an accompanying increased steric repulsion of the metal centers and alkoxo-ligands in the molecular structure of $[AnM_3(O^tBu)_7]$ (**AnM3**), causing an increase of the An–M distances.

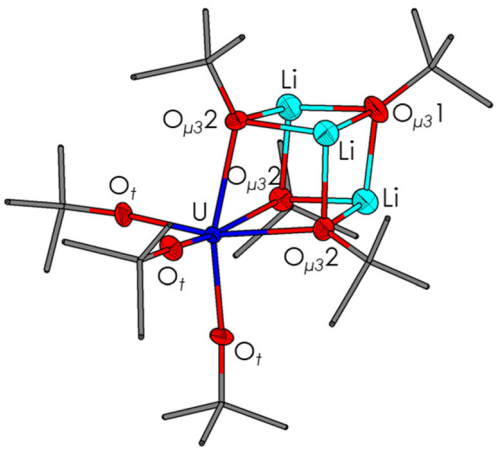

Fig. 1 Molecular structure of $[ULi_3(O^tBu)_7]$ (**ULi3**). Thermal ellipsoids are shown at the 50% probability level and hydrogen atoms have been omitted for clarity.

Fig. 2 shows the structural changes in the actinide–oxygen–alkali metal frameworks as a function of the metal ion size within the series of $[AnM_3(O^tBu)_7]$ derivatives **ULi3**, **ThLi3** and **ThNa3**. Increasing the ionic radius within the actinide series from Th^{IV} to U^{IV} only slightly affects the An–Li interatomic distance (**ULi3**: 3.243(7) Å, **ThLi3**: 3.29(2) Å), the Li–Li contact (**ULi3**: 2.460(9) Å; **ThLi3**: 2.43(2) Å) and slightly increases the An–O_t (**ULi3**: 2.120(3) Å; **ThLi3**: 2.193(6) Å) and An–$O_{\mu_3}2$ bond lengths (**ULi3**: 1.945(6) Å; **ThLi3**: 1.99(2) Å). In contrast, a significant metal–metal contact and M–O bond length change are observed upon varying the alkali metal ions. For the Li and Na derivatives **ThLi3** and **ThNa3**, the An–M distance (**ThLi3**: 3.29(2) Å; **ThNa3**: 3.606(3) Å), the M–M contact (**ThLi3**: 2.43(2) Å; **ThNa3**: 3.091(3) Å) and all M–O bonds were found to be elongated by ~0.3–0.4 Å. Additionally, the *tert*-butoxide octahedron surrounding the An^{IV} centers exhibited a higher degree of distortion for the smaller alkali metal ions, indicated by the *trans* O_t–An–$O_{\mu_3}2$ bond angle (**ThLi3**: 163.0(3)°; **ThNa3**: 166.6(1)°).

The room temperature ^1H and ^7Li NMR spectra of the actinide-lithium derivatives **ULi3** and **ThLi3** recorded in benzene-d_6 and toluene-d_8 showed a high complexity, with regard to the assignment of the signals to ligands observed in the solid-state structures. The ^1H NMR spectra showed 5 peaks in the range of −2.26 to 4.18 ppm for **ULi3** and 1.26 to 1.56 ppm for **ThLi3**, while the ^7Li NMR spectra exhibited 3 resonances in the range of −7.2 to 0.88 ppm for **ULi3** and 0.59 to 0.88 ppm for **ThLi3**. This is possibly due to the solution dynamics of the heterobimetallic compounds containing the smaller lithium cations and likely formation of different isomers in solution. The com-

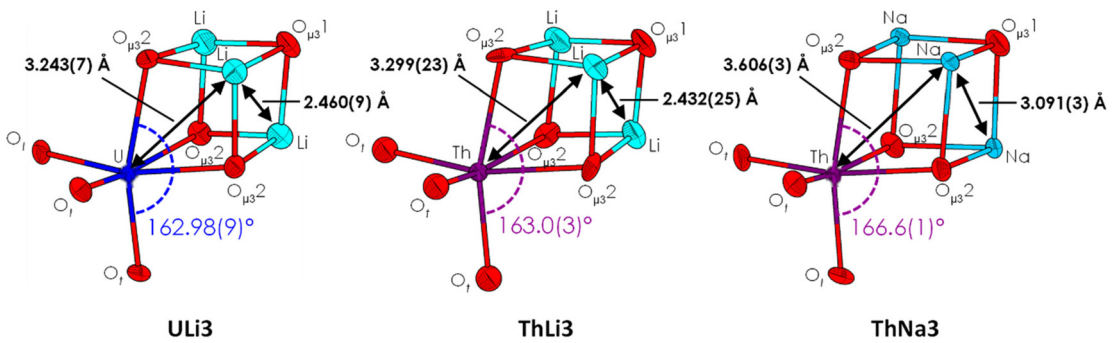

Fig. 2 The AnM_3O_7 skeletons of $[AnM_3(O^tBu)_7]$ (**ULi3**, **ThLi3**, **ThNa3**) with the corresponding An–M, M–M distances and the O_t–An–$O_{\mu_3}2$ (*trans*) angles. Thermal ellipsoids are shown at the 50% probability level and all hydrogen and carbon atoms have been omitted for clarity.

plexity of the spectra could not be reduced by low temperature measurement. A similar solution behavior based on NMR data was described by Hayton *et al.* for the uranium-lithium derivatives $[ULi_2(O^tBu)_6(THF)_2]$ (**ULi2-THF**) and $[U_2Li(O^tBu)_9(THF)]$ (**U2Li-THF**). In order to resolve the complex nature of the NMR spectra, a series of titration experiments with a varying amount of LiO^tBu were carried out.[23]

However, the ^{1}H NMR spectrum for the sodium derivative **ThNa3** in toluene-d_8 verified the cubane-type structure with two singlets at 1.19 and 1.42 ppm and an integrative ratio of 1 : 6. The resonance at 1.19 ppm is assigned to the μ_3-*tert*-butoxide group bridged among three sodium atoms, whereas the resonance at 1.42 ppm includes three *tert*-butoxides surrounding the Th center and three *tert*-butoxide group bridging Th and Na centers. A ^{23}Na NMR spectrum recorded in toluene-d_8 confirmed the structural integrity of **ThNa3** in solution, with one resonance observed at 5.07 ppm for the three chemically equivalent μ_3-bridged sodium cations.

$[AnM_2(O^tBu)_6]$ derivatives (AnM2)

When compared to the previously reported $[ULi_2(O^tBu)_6(THF)]$[23] (**ULi2-THF**), the alkali metal centers in this study are not coordinated by any additional Lewis basic ligand, such as THF (Fig. 3). The use of a coordinating solvent substantially influences the structural motif of the resulting complex both in the solid state and in solution, as the formation of the above-mentioned **AnLi3** structure is apparently suppressed by the coordination of one THF molecule to both Li^I-centers each.

The actinide centers in the series of compounds **UNa2**, **ThK2**, **UK2**, **ThRb2**, **URb2**, **ThCs2** and **UCs2** were coordinated by six *tert*-butoxide ligands in a distorted octahedral fashion (Fig. 3), similar to the **ULi2-THF** complex.[23] Two of these *tert*-butoxide ligands are bound terminally (O_t) to the actinide center, whereas the two monovalent alkali metals are coordinated by alkoxide groups bridging to the An^{IV} center in bidentate ($2 \times O_{\mu_2}$) and tridentate ($2 \times O_{\mu_3}$) modes. Thus, the structure exhibits a framework of two face-shared $[AnMO_3]$ trigonal bipyramids, with one actinide center, one alkali metal center, one μ_2-bridged and two μ_3-bridged *tert*-butoxide ligands occupying the corners of each tetrahedron.

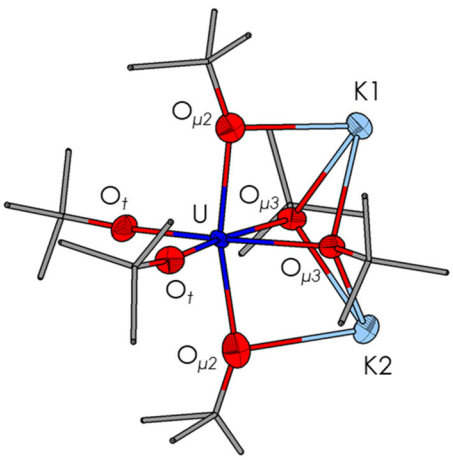

Fig. 3 The molecular structure of $[UK_2(O^tBu)_6]$ (**UK2**). Thermal ellipsoids are shown at the 50% probability level. All hydrogen atoms and a disordered part of the molecule (9%) as well as a free solvent molecule have been omitted for clarity.

The An^{IV}–O_t bond lengths are in good agreement with the respective bonds in reported An^{IV} (Th, U) *tert*-butoxide structures.[23,34,35] A comparison of the uranium–alkali metal compounds **UNa2–UCs2** and the known uranium-lithium derivative **ULi2-THF**[23] revealed that the size of the alkali metal ion affected the An–M distance that showed an increasing trend with increasing size of the cations (2.87(1) Å **ULi2-THF**;[23] 3.193(2) Å **UNa2**; 3.525(1) Å **UK2**; 3.656(3) Å **URb2**; 3.8754(9) Å **UCs2**) and M–M distance (2.89(3) Å **ULi2-THF**;[23] 3.453(3) Å **UNa2**; 4.043(3) Å **UK2**; 4.188(7) Å **URb2**; 4.6564(9) Å **UCs2**) (Fig. 4).

Moreover, the M–O bonds were found to be elongated with increasing size of the monovalent alkali metal ion (Table S4†). A comparison of the O_{μ_3}–An–O_{μ_3} *trans* bond angles indicated a higher distortion of the An^{IV} octahedron for derivatives with smaller alkali metals. A higher distortion goes along with a decrease of the An–O_t bond length, since more space is provided for the terminal *tert*-butoxide groups, and an increase of the An–O_{μ_3} bond length as a consequence of a higher steric repulsion of the alkoxide ligands. In the **AnM2** molecular structures, a benzene ring was found to be located near one of the alkali metals that seems to be a solvent incorporation and no π-coordination based on the distances towards the alkali metal and the fact that it is only located towards one of two available alkali metals. However, the hydrogen atoms on a methyl group of the bidentate bridged *tert*-butoxides of compound **ThK2** show agostic interactions (K–H distances of 1.925(7) Å and K–C distances of 2.3(7) Å) with the alkali metal without the localized benzene molecule, whereas anagostic interactions (K–H distances of 2.67(8) Å and K–C distances of 3.4(3) Å) with the alkali metal localized by a benzene molecule are present (ESI-Fig. S20†).

The ^{1}H NMR spectra of the **UM2**-type structures in benzene-d_6 showed high complexity due to the paramagnetism of U^{IV}. The recorded spectra showed several sharp singlets in the range of −3.01 to 17.39 ppm and one broad signal at 1.67 ppm. Attempts to use another deuterated non-polar hydrocarbon solvent were not conclusive. For instance, the ^{1}H NMR spectrum of **UNa2** in toluene-d_8 merely showed two signals at −3.03 and 17.36 ppm, which are also observed in the spectrum recorded in benzene-d_6; however the broad signal at 1.67 ppm was not observed. Although **UNa2** revealed one resonance in the ^{23}Na NMR spectra in toluene-d_8 at 32.89 ppm, supporting the existence of the **UM2**-type structure with two chemically equivalent μ_3-bridged Na^I-centers, the ^{1}H NMR signals and their integrative ratios were not assignable to the **UM2**-type structure.

However, the ^{1}H NMR spectrum of the diamagnetic thorium derivatives **ThK2**, **ThRb2** and **ThCs2** in benzene-d_6 revealed a single resonance at 1.51, 1.55 and 1.58 ppm,

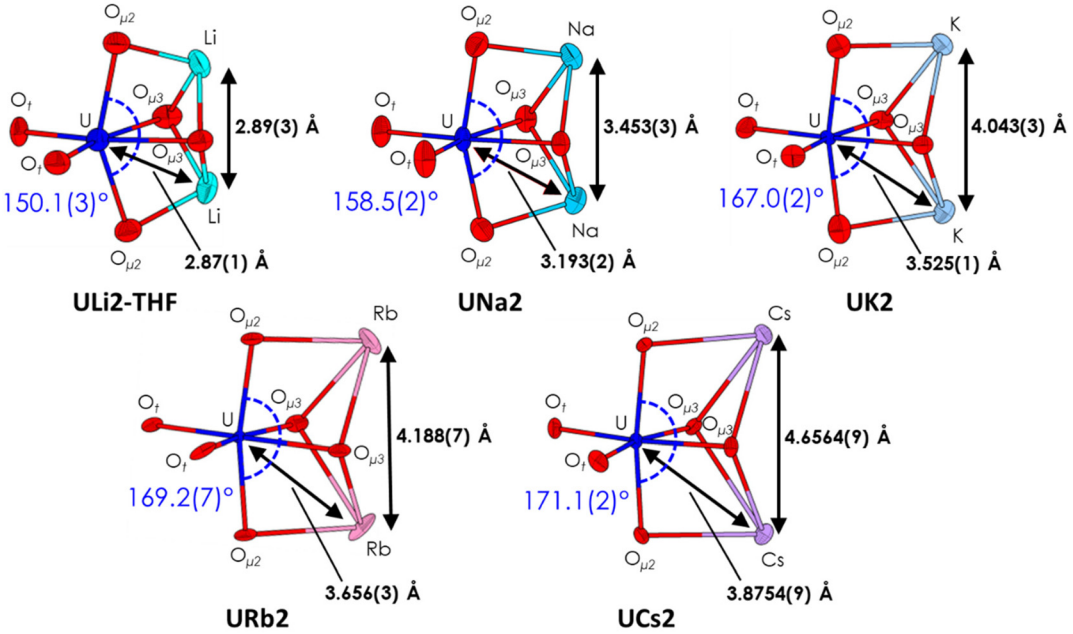

Fig. 4 The AnM_2O_6 skeletons of $[ULi_2(O^tBu)_6(THF)_2]$[23] (**ULi2-THF**) and $[AnM_2(O^tBu)_6]$ (**UNa2**, **UK2**, **URb2**, **UCs2**) with the corresponding An–M and M–M distances and the O_t–An–$O_{\mu_3}2$ (*trans*) angles. Thermal ellipsoids are shown at the 50% probability level and all hydrogen and carbon atoms have been omitted for clarity.

respectively, which were unambiguously assigned to the six *tert*-butoxide ligands surrounding the thorium center, namely the O_t terminal, O_{μ_2} μ_2-bridged and O_{μ_3} μ_3-bridged *tert*-butoxide ligands.

Furthermore, both structures **AnM2** and **AnM3** were investigated by IR spectroscopy that exhibited mainly comparable peak patterns in both cases; however, the IR spectra of **AnM2** and **AnM3** differentiated in one additional IR band observed at ~670–690 and ~450–480 cm^{-1}, respectively (see ESI, Fig. S18 and S19†).

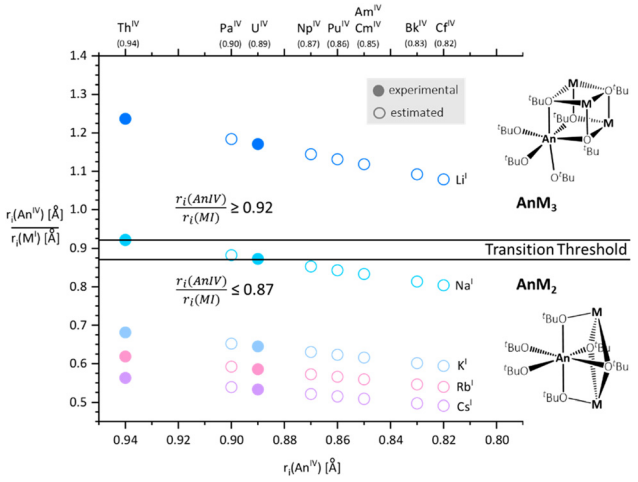

Fig. 5 Diagram for the proposed An^{IV} and M^I metal ion size (C.N. 6) dependent structural outcome of the $[AnM_3(O^tBu)_7]$ (**AnM3**) and $[AnM_2(O^tBu)_6]$ (**AnM2**) structure type, including the $r_i(An^{IV})/r_i(M^I)$ values of the **AnM3** and **AnM2** (An^{IV} = Th, U) structures.

Conclusions

A general synthetic strategy for heterobimetallic An^{IV}–M^I *tert*-butoxides (An^{IV} = Th, U; M^I = Li, Na, K, Rb, Cs) was established through simple ligand exchange of alkali metals and actinide silyl amides in *tert*-butyl alcohol in non-polar hydrocarbon solvents. The targeted formation of $[AnM_3(O^tBu)_7]$ (**AnM3**-type: **ULi3**, **ThLi3**, **ThNa3**) and $[AnM_2(O^tBu)_6]$ (**AnM2**-type: **UNa2**, **UK2**, **ThK2**, **URb2**, **ThRb2**, **UCs2**, **ThCs2**) was simply controlled by the variation of the An^{IV} and M^I ionic radii and was found to be independent of a 1 : 3 or 1 : 2 (An^{IV} : M^I) stoichiometry in the reactions. The ratio of the ionic radii[40] $r_i(An^{IV})/r_i(M^I)$ allowed us to estimate the threshold values, limiting the formation of structures with 1 : 2 (**AnM2**) or 1 : 3 (**AnM3**) ratios. A ratio of 0.92 or higher was found to favor the **AnM3** framework, whereas the **AnM2** structure was obtained for values below 0.87. The transition threshold for both structures is located in between the ratio of 0.87 and 0.92, which are the corresponding ratio values of **UNa2** and **ThNa3**, respectively. The respective ratios were calculated for all tetravalent actinides against all monovalent alkali metals as depicted in Fig. 5.

These values deliver predictions if the **AnM2** or **AnM3** structure-type is obtained when an equivalent of actinide precursor [AnN′N″] (An^{IV} = Th, Pa, U, Np, Am, Cm, Bk, Cf) is treated with 2 or 3 eq. or an excess of [MN″] (M^I = Li, Na, K, Rb, Cs) and HO^{t}Bu for the available tetravalent actinides and monovalent alkali metals.

Experimental section

All reactions were performed under inert conditions in a glovebox with an argon atmosphere and less than 0.1 ppm H_2O and O_2 or using standard Schlenk techniques. Chemicals were obtained from Sigma-Aldrich Chemical Co., Acros Organics, Alfa Aesar, VWR, Fischer Scientific and Strem Chemical Co. Solvents and alcohols were dried over sodium and distilled prior to use. After degassing with the freeze–pump–thaw technique, it was brought into the glovebox and stored over dried molecular sieves (3 Å). The metal silyl amides [MN″] (M^I = Li,[41] Rb,[42] Cs[43]) and the metallacycle [AnN′N″] (An^{IV} = Th, U)[44] were synthesized according to the literature methods. The [MN″] (M^I = Na, K) derivatives were purchased from Sigma Aldrich and purified by sublimation under reduced pressure (10^{-3} mbar for M^I = Li, Na, K, Rb, Cs; 10^{-6} mbar for An^{IV} = Th, U) prior to use.

SXRD data were obtained by mounting a suitable single crystal on a MiTiGen Microloop™ and attaching this to the goniometer head of an SC-XRD Bruker D8 Venture. The crystal was cooled to 100–120 K using an Oxford Cryostream low temperature device. The full dataset was recorded and the images were processed using APEX2. Structure solution by direct methods was achieved using SHELXS programs, and the structural model was refined by full matrix least squares on F^2 using SHELX97. Molecular graphics were plotted using Diamond. Editing of CIFs and construction of tables and bond lengths and angles was achieved using PLATON and Olex2.

The NMR spectra were recorded on a Bruker Avance 300 in benzene-d_6 at 298 K. Additional NMR spectra were recorded on a Bruker Avance II 300, Bruker Avance 400 or Bruker Avance III 500 spectrometer. The ^{1}H (300.1 MHz), ^{1}H (400.1 MHz), ^{1}H (500.1 MHz), ^{7}Li (116.6 MHz), ^{23}Na (132.3 MHz) chemical shifts are reported in parts per million (ppm) relative to external tetramethylsilane and are referenced internally to the proton impurity of the solvent. For characterization of the observed signal multiplicities, the following abbreviations were used: s (singlet) as well as br (broad). The NMR spectra were analyzed with the software Bruker Topspin 4.1.1.

Infrared spectra were obtained using a Platinum ATR Spectrometer on a crystal plate with samples analyzed using OPUS software. The spectrometer is placed in an argon glovebox.

Elemental analyses were carried out on a HEKAtech CHNS Euro EA 3000. The sample preparation was performed in a glove box, whereas the reweighing of the cartridges was done outside under environmental atmosphere.

According to the German legislation, natural uranium/thorium, used in this work, is not classified as "radioactive", but merely as a chemical element in its natural isotopic composition, since the total inventory of natural uranium and thorium in the laboratory does not exceed 100 grams and 200 grams, respectively. Hence, no additional precautions were necessary, and the uranium/thorium precursor was handled and stored taking similar precautions to those applicable to any hazardous heavy metal compound.

General procedure for $[AnM_3(O^tBu)_7]$ (AnM3)

A mixture of 1.0 eq. of $[An\{(CH_2SiMe_2)N(SiMe_3)_2\}\{N(SiMe_3)_2\}_2]$ and 3.0 eq. of $[M\{N(SiMe_3)_2\}]$ in benzene was treated with 7.0 eq. of *tert*-butanol. The mixture was stirred for 1 d at room temperature. After slow evaporation of all volatiles at room temperature, crystals of $[AnM_3(O^tBu)_7]$ were obtained.

Synthesis of $[ULi_3(O^tBu)_7]$ (ULi3)

15.0 mg (20.9 μmol) of $[U\{(CH_2SiMe_2)N(SiMe_3)_2\}\{N(SiMe_3)_2\}_2]$, 10.5 mg (62.7 μmol) of $[Li\{N(SiMe_3)_2\}]$ and 10.8 mg (146.2 μmol) of *tert*-butanol were reacted to obtain $[ULi_3(O^tBu)_7]$ (**ULi3**) in the form of bright blue crystals in a nearly quantitative yield of 15.6 mg (96%). ^{1}H NMR (500 MHz, 25 °C, C_6D_6): δ −2.22 (s), δ 1.19 (s), δ 1.28 (s), δ 3.36 (s), δ 4.17 (s). ^{1}H NMR (500 MHz, 25 °C, C_7D_8): δ −2.23 (s), δ 1.21 (s), δ 1.31 (s), δ 3.41 (s), δ 4.19 (s). ^{7}Li NMR (117 MHz, 25 °C, C_6D_6): δ −7.20 (s), δ −6.21 (s), δ 0.88 (s). IR (cm^{-1}): 2966 (m), 2867 (w), 1470 (w), 1385 (w), 1357 (m), 1208 (m), 1188 (s), 972 (s), 946 (s), 839 (w), 761 (m), 582 (m), 498 (s), 480 (s). Anal. calcd $ULi_3O_7C_{28}H_{63}$: C 43.64, H 8.24. Found: C 44.13, H 7.97.

Synthesis of $[ThLi_3(O^tBu)_7]$ (ThLi3)

15.0 mg (21.1 μmol) of $[Th\{(CH_2SiMe_2)N(SiMe_3)_2\}\{N(SiMe_3)_2\}_2]$, 10.6 mg (63.2 μmol) of $[Li\{N(SiMe_3)_2\}]$ and 10.9 mg (147.4 μmol) of *tert*-butanol were reacted to obtain $[ThLi_3(O^tBu)_7]$ (**ThLi3**) in the form of colorless crystals in a nearly quantitative yield of 15.8 mg (98%). ^{1}H NMR (500 MHz, 25 °C, C_6D_6): δ 1.28 (s), δ 1.33 (s), δ 1.49 (s), δ 1.54 (s), δ 1.56 (s). ^{1}H NMR (500 MHz, 25 °C, C_7D_8): δ 1.26 (s), δ 1.30 (s), δ 1.46 (s), δ 1.52 (s), δ 1.53 (s). ^{7}Li NMR (117 MHz, 25 °C, C_6D_6): δ 0.59 (s), δ 0.73 (s), δ 0.88 (s, *Li*–OC$(CH_3)_3$). IR (cm^{-1}): 2970 (m), 2931 (m), 2865 (w), 1472 (w), 1385 (w), 1359 (m), 1209 (s), 1190 (s), 967 (s), 946 (s), 901 (m), 757 (m), 579 (m), 494 (s), 480 (s). Anal. calcd $ThLi_3O_7C_{28}H_{63}$: C 43.98, H 8.30. Found: C 44.89, H 8.94.

Synthesis of $[ThNa_3(O^tBu)_7]$ (ThNa3)

15.0 mg (21.1 μmol) of $[Th\{(CH_2SiMe_2)N(SiMe_3)_2\}\{N(SiMe_3)_2\}_2]$, 11.6 mg (63.2 μmol) of $[Na\{N(SiMe_3)_2\}]$ and 10.9 mg (147.4 μmol) of *tert*-butanol were reacted to obtain $[ThNa_3(O^tBu)_7]$ (**ThNa3**) in the form of colorless crystals in a nearly quantitative yield of 16.5 mg (96%). ^{1}H NMR (500 MHz, 25 °C, C_7D_8): δ 1.29 (μ_3-bridged Na_3–OC$(CH_3)_3$, s, 9H), δ 1.42 (μ_3-bridged U–Na_2–OC$(CH_3)_3$ & terminal U–OC$(CH_3)_3$, s, 54H). ^{23}Na NMR (132 MHz, 25 °C, C_7D_8): δ 5.05 (μ_3-bridged Na, s, 3Na). IR (cm^{-1}): 2967 (w), 2860 (w), 1474 (w), 1382 (w), 1353 (m), 1195 (s), 948 (s), 833 (w), 761 (m), 542 (w), 481 (s), 435 (m). Anal. calcd $ThNa_3O_7C_{28}H_{63}$: C 41.38, H 7.81. Found: C 42.62, H 7.59.

General reaction procedure for $[AnM_2(O^tBu)_6]$ (AnM2)

A mixture of 1.0 eq. of $[An\{(CH_2SiMe_2)N(SiMe_3)_2\}\{N(SiMe_3)_2\}_2]$ and 2.0 eq. of $[M\{N(SiMe_3)_2\}]$ in benzene was treated with 6.0 eq. of *tert*-butanol. The mixture was stirred for 1 d at room

temperature. After slow evaporation of all volatiles at room temperature, crystals of $[AnM_3(O^tBu)_7]$ were obtained.

Synthesis of $[UNa_2(O^tBu)_6]$ (UNa2)

15.0 mg (20.9 μmol) of $[U\{(CH_2SiMe_2)N(SiMe_3)_2\}\{N(SiMe_3)_2\}_2]$, 7.7 mg (41.8 μmol) of $[Na\{N(SiMe_3)_2\}]$ and 9.3 mg (125.3 μmol) of *tert*-butanol were reacted to obtain $[UNa_2(O^tBu)_6]$ (**UNa2**) in the form of blue crystals in a nearly quantitative yield of 16.2 mg (97%). ^{1}H NMR (300 MHz, 25 °C, C_6D_6): δ −3.02 (s), δ 0.10 (s), δ 1.38 (s), δ 1.67 (br), δ 17.36 (s). ^{1}H NMR (500 MHz, 25 °C, C_7D_8): δ −3.04 (s), δ 17.34 (s). ^{23}Na NMR (132 MHz, 25 °C, C_7D_8): δ 32.89 (μ_3-bridged Na, s, 2Na). IR (cm^{-1}): 2960 (m), 2905 (w), 2868 (w), 1472 (w), 1380 (w), 1355 (m), 1221 (m), 1192 (s), 1008 (w), 948 (s), 899 (m), 761 (m), 692 (m), 478 (s). Anal. calcd $UNa_2O_6C_{30}H_{60}$: C 45.00, H 7.55. Found: C 43.86, H 8.01.

Synthesis of $[UK_2(O^tBu)_6]$ (UK2)

15.0 mg (20.9 μmol) of $[U\{(CH_2SiMe_2)N(SiMe_3)_2\}\{N(SiMe_3)_2\}_2]$, 8.3 mg (41.8 μmol) of $[K\{N(SiMe_3)_2\}]$ and 9.3 mg (125.3 μmol) of *tert*-butanol were reacted to obtain $[UK_2(O^tBu)_6]$ (**UK2**) in the form of blue crystals in a nearly quantitative yield of 17.1 mg (98%). ^{1}H NMR (300 MHz, 25 °C, C_6D_6): δ −1.55 (s), δ 1.68 (s), δ 2.04 (s), δ 2.56 (s), δ 3.12 (s), δ 14.42 (s). IR (cm^{-1}): 2960 (w), 2899 (w), 2864 (w), 1482 (w), 1380 (w), 1353 (m), 1215 (m), 1193 (s), 1008 (w), 949 (s), 764 (w), 691 (m), 478 (s), 409 (w). Anal. calcd $UK_2O_6C_{30}H_{60}$: C 43.26, H 7.26. Found: C 43.91, H 7.02.

Synthesis of $[URb_2(O^tBu)_6]$ (URb2)

15.0 mg (20.9 μmol) of $[U\{(CH_2SiMe_2)N(SiMe_3)_2\}\{N(SiMe_3)_2\}_2]$, 10.3 mg (41.8 μmol) of $[Rb\{N(SiMe_3)_2\}]$ and 9.3 mg (125.3 μmol) of *tert*-butanol were reacted to obtain $[URb_2(O^tBu)_6]$ (**URb2**) in the form of blue crystals in a nearly quantitative yield of 19.0 mg (98%). ^{1}H NMR (300 MHz, 25 °C, C_6D_6): δ −2.71 (s), δ −1.79 (s), δ 1.67 (s), δ 2.61 (s), δ 4.07 (s), δ 16.20 (s). IR (cm^{-1}): 2953 (w), 2899 (w), 2865 (w), 1484 (w), 1460 (w), 1380 (w), 1353 (w), 1193 (s), 1010 (w), 946 (s), 760 (w), 689 (m), 476 (s), 408 (w). Anal. calcd $URb_2O_6C_{30}H_{60}$: C 38.92, H 6.53. Found: C 37.89, H 6.75.

Synthesis of $[UCs_2(O^tBu)_6]$ (UCs2)

15.0 mg (20.9 μmol) of $[U\{(CH_2SiMe_2)N(SiMe_3)_2\}\{N(SiMe_3)_2\}_2]$, 12.2 mg (41.8 μmol) of $[Cs\{N(SiMe_3)_2\}]$ and 9.3 mg (125.3 μmol) of *tert*-butanol were reacted to obtain $[UCs_2(O^tBu)_6]$ (**UCs2**) in the form of blue crystals in a nearly quantitative yield of 21.3 mg (96%). ^{1}H NMR (400 MHz, 25 °C, C_6D_6): δ −6.48 (s), δ −5.08 (s), δ 1.18 (s), 2.11 (s), 5.51 (s), 5.91 (s). IR (cm^{-1}): 2966 (m), 2930 (w), 2907 (w), 2874 (w), 1465 (w), 1383 (w), 1359 (m), 1224 (m), 1184 (s), 980 (m), 945 (s), 900 (s), 837 (w), 766 (m), 692 (w), 494 (s), 475 (s). Anal. calcd $UCs_2O_6C_{33}H_{63}$: C 37.40, H 5.99. Found: C 36.87, H 6.32.

Synthesis of $[ThK_2(O^tBu)_6]$ (ThK2)

15.0 mg (21.1 μmol) of $[Th\{(CH_2SiMe_2)N(SiMe_3)_2\}\{N(SiMe_3)_2\}_2]$, 8.4 mg (42.2 μmol) of $[K\{N(SiMe_3)_2\}]$ and 9.3 mg (125.3 μmol) of *tert*-butanol were reacted to obtain $[ThK_2(O^tBu)_6]$ (**ThK2**) in the form of colorless crystals in a nearly quantitative yield of 16.9 mg (97%). ^{1}H NMR (300 MHz, 25 °C, C_6D_6): δ 1.51 (μ_3-bridged OC(CH_3)$_3$ & μ_2-bridged OC(CH_3)$_3$ & terminal U-OC(CH_3)$_3$, s, 54H). IR (cm^{-1}): 2960 (w), 2899 (w), 2861 (w), 1484 (w), 1457 (w), 1379 (w), 1353 (m), 1196 (s), 1013 (w), 954 (s), 755 (w), 691 (m), 478 (s). Anal. calcd $ThK_2O_6C_{30}H_{60}$: C 43.57, H 7.31. Found: C 44.74, H 6.67.

Synthesis of $[ThRb_2(O^tBu)_6]$ (ThRb2)

15.0 mg (21.1 μmol) of $[Th\{(CH_2SiMe_2)N(SiMe_3)_2\}\{N(SiMe_3)_2\}_2]$, 10.4 mg (42.2 μmol) of $[Rb\{N(SiMe_3)_2\}]$ and 9.3 mg (125.3 μmol) of *tert*-butanol were reacted to obtain $[ThRb_2(O^tBu)_6]$ (**ThRb2**) in the form of colorless crystals in a nearly quantitative yield of 18.4 mg (95%). ^{1}H NMR (300 MHz, 25 °C, C_6D_6): δ 1.55 (μ_3-bridged OC(CH_3)$_3$ & μ_2-bridged OC(CH_3)$_3$ & terminal U–OC(CH_3)$_3$, s, 54H). IR (cm^{-1}): 2953 (s), 2895 (w), 2864 (w), 1484 (w), 1460 (w), 1380 (w), 1353 (m), 1195 (s), 1011 (w), 953 (s), 755 (w), 687 (m), 476 (s). Anal. calcd $ThRb_2O_6C_{30}H_{60}$: C 39.18, H 6.58. Found: C 38.73, H 6.34.

Synthesis of $[ThCs_2(O^tBu)_6]$ (ThCs2)

15.0 mg (21.1 μmol) of $[Th\{(CH_2SiMe_2)N(SiMe_3)_2\}\{N(SiMe_3)_2\}_2]$, 12.4 mg (42.2 μmol) of $[Cs\{N(SiMe_3)_2\}]$ and 9.3 mg (125.3 μmol) of *tert*-butanol were reacted to obtain $[ThCs_2(O^tBu)_6]$ (**ThCs2**) in the form of colorless crystals in a nearly quantitative yield of 21.0 mg (98%). ^{1}H NMR (300 MHz, 25 °C, C_6D_6): δ 1.58 (μ_3-bridged OC(CH_3)$_3$ & μ_2-bridged OC(CH_3)$_3$ & terminal U–OC(CH_3)$_3$, s, 54H). IR (cm^{-1}): 2966 (m), 2933 (w), 2871 (w), 1470 (w), 1382 (w), 1357 (m), 1191 (s), 952 (s), 934 (s), 839 (m), 790 (m), 767 (m), 689 (w), 585 (w), 480 (s). Anal. calcd $ThCs_2O_6C_{30}H_{60}$: C 35.51, H 5.96. Found: C 34.98, H 5.71.

Conflicts of interest

There are no conflicts to declare.

Acknowledgements

The authors cordially thank Dr Carsten Lenczyk and Dr Tobias Stürzer, both Bruker AXS Karlsruhe, for additional crystallographic advice and support, providing us with preliminary models for the modulated dataset **URb2**, the inversion twin dataset of **ThNa3** and the merohedral twin dataset of **ThCs2**. We also thank Mr Dirk Pullem, University of Cologne, for CHNS measurements.

References

1 D. C. Bradley, Metal alkoxides and dialkylamides, in *Advances in inorganic chemistry and radiochemistry*, Elsevier, 1972, vol. 15, pp. 259–322.

2 S. M. Guillaume, Recent advances in ring-opening polymerization strategies toward α, ω-hydroxy telechelic polyesters and resulting copolymers, *Eur. Polym. J.*, 2013, **49**(4), 768–779.
3 M. Hatano and K. Ishihara, Lanthanum(III) catalysts for highly efficient and chemoselective transesterification, *Chem. Commun.*, 2013, **49**(20), 1983–1997.
4 A. Tsubouchi, D. Muramatsu and T. Takeda, Copper(I)–Catalyzed Alkylation of Aryl–and Alkenylsilanes Activated by Intramolecular Coordination of an Alkoxide, *Angew. Chem., Int. Ed.*, 2013, **52**(48), 12719–12722.
5 T. D. Manning, Y. F. Loo, A. C. Jones, H. C. Aspinall, P. R. Chalker, J. F. Bickley, L. M. Smith and G. W. Critchlow, Deposition of LaAlO3 films by liquid injection MOCVD using a new [La–Al] single source alkoxide precursor, *J. Mater. Chem.*, 2005, **15**(33), 3384–3387.
6 S. Mathur, M. Veith, V. Sivakov, H. Shen, V. Huch, U. Hartmann and H. B. Gao, Phase–Selective Deposition and Microstructure Control in Iron Oxide Films Obtained by Single–Source CVD, *Chem. Vap. Deposition*, 2002, **8**(6), 277–283.
7 A. Jamil, J. Schlafer, Y. Gonullu, A. Lepcha and S. Mathur, Precursor-Derived Rare Earth Metal Pyrochlores: Nd2Sn2O7 Nanofibers and Thin Films As Efficient Photoabsorbers, *Cryst. Growth Des.*, 2016, **16**(9), 5260–5267.
8 S. Mathur, S. Barth, U. Werner, F. Hernandez-Ramirez and A. Romano-Rodriguez, Chemical Vapor Growth of One–dimensional Magnetite Nanostructures, *Adv. Mater.*, 2008, **20**(8), 1550–1554.
9 S. Mathur, T. Ruegamer and I. Grobelsek, Phase–Selective CVD of Vanadium Oxide Nanostructures, *Chem. Vap. Deposition*, 2007, **13**(1), 42–47.
10 A. Raauf, J. Leduc, M. Frank, D. Stadler, D. Graf, M. Wilhelm, M. Grosch and S. Mathur, Magnetic Field-Assisted Chemical Vapor Deposition of UO2 Thin Films, *Inorg. Chem.*, 2021, **60**(3), 1915–1921.
11 A. Raauf, J. Schläfer, I. Gessner, A. Lichtenberg, M. Zegke, T. Fischer and S. Mathur, Homo-and heteroleptic lanthanide-iron alkoxides as precursors in materials synthesis, *J. Indian Chem. Soc.*, 2022, 100347.
12 D. Bradley, A. K. Chatterjee and A. K. Chatterjee, Sexavalent compounds of uranium—I: Uranyl alkoxides and uranium hexa-alkoxides, *J. Inorg. Nucl. Chem.*, 1959, **12**(1–2), 71–78.
13 D. Bradley and H. Holloway, Metal oxide alkoxide polymers: part V. The hydrolysis of some alkoxides of tin(IV), CERIUM (IV), AND URANIUM(V), *Can. J. Chem.*, 1962, **40**(6), 1176–1182.
14 D. Bradley, R. Kapoor and B. Smith, 30. Organosiloxy-derivatives of metals. Part II. Trialkylsilyloxides of quinquevalent and sexivalent uranium, *J. Chem. Soc.*, 1963, 204–207.
15 D. Bradley, R. Kapoor and B. Smith, Alkoxides of uranium (IV), *J. Inorg. Nucl. Chem.*, 1962, **24**(7), 863–867.
16 R. Jones, G. Karmas, G. Martin Jr. and H. Gilman, Organic compounds of Uranium. II. Uranium(IV) amides, alkoxides and mercaptides, *J. Am. Chem. Soc.*, 1956, **78**(17), 4285–4286.
17 R. Jones, E. Bindschadler, D. Blume, G. Karmas, G. Martin Jr., J. Thirtle and H. Gilman, Organic Compounds of Uranium. V. Derivatives of Uranium(V) Alkoxides, *J. Am. Chem. Soc.*, 1956, **78**(23), 6027–6030.
18 R. Jones, E. Bindschadler, G. Karmas, G. Martin Jr., J. Thirtle, F. Yoeman and H. Gilman, Organic compounds of uranium. IV. Uranium(V) alkoxides, *J. Am. Chem. Soc.*, 1956, **78**(17), 4289–4290.
19 R. Jones, E. Bindschadler, D. Blume, G. Karmas, G. Martin Jr., J. Thirtle, F. Yeoman and H. Gilman, Organic compounds of uranium. VI. Uranium(VI) alkoxides, *J. Am. Chem. Soc.*, 1956, **78**(23), 6030–6032.
20 R. Jones, E. Bindschadler, G. Martin Jr., J. Thirtle and H. Gilman, Organic Compounds of Uranium. VII. Uranyl Alkoxides and Dithiocarbamates, *J. Am. Chem. Soc.*, 1957, **79**(18), 4921–4922.
21 W. G. Van der Sluys, A. P. Sattelberger and M. W. McElfresh, Uranium alkoxide chemistry V. Synthesis, characterization and interconversion of uranium(IV) tert-butoxide complexes, *Polyhedron*, 1990, **9**(15–16), 1843–1848.
22 W. Van der Sluys and A. Sattelberger, Actinide alkoxide chemistry, *Chem. Rev.*, 1990, **90**(6), 1027–1040.
23 S. Fortier, G. Wu and T. W. Hayton, Synthesis and Characterization of Three Homoleptic Alkoxides of Uranium:[Li (THF)] 2 [UIV (O t Bu) 6],[Li (Et_2O)][UV (O t Bu) 6], and UVI (O t Bu) 6, *Inorg. Chem.*, 2008, **47**(11), 4752–4761.
24 T. Monde, H. Kozuka and S. Sakka, Superconducting oxide thin films prepared by sol–gel technique using metal alkoxides, *Chem. Lett.*, 1988, **17**(2), 287–290.
25 J. Livage and C. Sanchez, Sol-gel chemistry, *J. Non-Cryst. Solids*, 1992, **145**, 11–19.
26 K. Murty and I. Charit, Structural materials for Gen-IV nuclear reactors: Challenges and opportunities, *J. Nucl. Mater.*, 2008, **383**(1–2), 189–195.
27 P. Makowski, X. Deschanels, A. Grandjean, D. Meyer, G. Toquer and F. Goettmann, Mesoporous materials in the field of nuclear industry: applications and perspectives, *New J. Chem.*, 2012, **36**(3), 531–541.
28 G. L. Murphy, E. M. Langer, O. Walter, Y. Wang, S. Wang and E. V. Alekseev, Insights into the structural chemistry of anhydrous and hydrous hexavalent uranium and neptunium dinitrato, trinitrato, and tetranitrato complexes, *Inorg. Chem.*, 2020, **59**(10), 7204–7215.
29 G. Murphy, B. J. Kennedy, B. Johannessen, J. A. Kimpton, M. Avdeev, C. S. Griffith, G. J. Thorogood and Z. Zhang, Structural studies of the rhombohedral and orthorhombic monouranates: CaUO4, α-SrUO4, β-SrUO4 and BaUO4, *J. Solid State Chem.*, 2016, **237**, 86–92.
30 G. L. Murphy, P. Kegler, Y. Zhang, Z. Zhang, E. V. Alekseev, M. D. de Jonge and B. J. Kennedy, High-pressure synthesis, structural, and spectroscopic studies of the Ni–U–O system, *Inorg. Chem.*, 2018, **57**(21), 13847–13858.

31 G. L. Murphy, C.-H. Wang, Z. Zhang, P. M. Kowalski, G. Beridze, M. Avdeev, O. Muransky, H. E. Brand, Q.-F. Gu and B. J. Kennedy, Controlling oxygen defect formation and its effect on reversible symmetry lowering and disorder-to-order phase transformations in nonstoichiometric ternary uranium oxides, *Inorg. Chem.*, 2019, **58**(9), 6143–6154.

32 G. B. Jin, J. Lin, S. L. Estes, S. Skanthakumar and L. Soderholm, Influence of countercation hydration enthalpies on the formation of molecular complexes: a Thorium–nitrate example, *J. Am. Chem. Soc.*, 2017, **139**(49), 18003–18008.

33 M. Veith, S. Mathur and C. Mathur, New perspectives in the tailoring of hetero (bi-and tri-) metallic alkoxide derivatives, *Polyhedron*, 1998, **17**(5–6), 1005–1034.

34 F. A. Cotton, D. O. Marler and W. Schwotzer, Dinuclear uranium alkoxides. Preparation and structures of KU2 (OCMe3) 9, U2 (OCMe3) 9, and U2 (OCHMe2) 10, containing [uranium(IV), uranium(IV)],[uranium(IV), uranium(V)], and [uranium(V), uranium(V)], respectively, *Inorg. Chem.*, 1984, **23**(25), 4211–4215.

35 D. L. Clark and J. G. Watkin, Synthesis and characterization of thorium tert-butoxide complexes: X-ray crystal structures of Th (O-tert-Bu) 4 (py) 2 and NaTh2 (O-tert-Bu) 9, *Inorg. Chem.*, 1993, **32**(9), 1766–1772.

36 E. Weiss, H. Alsdorf, H. Kühr and H.-F. Grützmacher, Röntgenographische, NMR-und massenspektrometrische Untersuchungen der tert.-Butylate des Kaliums, Rubidiums und Caesiums, *Chem. Ber.*, 1968, **101**(11), 3777–3786.

37 A. Jamil, J. Schläfer, Y. Gönüllü, A. Lepcha and S. Mathur, Precursor-derived rare earth metal pyrochlores: Nd2Sn2O7 nanofibers and thin films as efficient photoabsorbers, *Cryst. Growth Des.*, 2016, **16**(9), 5260–5267.

38 J. F. Allan, R. Nassar, E. Specht, A. Beatty, N. Calin and K. W. Henderson, Characterization of a kinetically stable, highly ordered, octameric form of lithium tert-butoxide and its implications regarding aggregate formation, *J. Am. Chem. Soc.*, 2004, **126**(2), 484–485.

39 H. Nekola, F. Olbrich and U. Behrens, Kristall–und Molekülstrukturen von Lithium–und Natrium–tert–butoxid, *Z. Anorg. Allg. Chem.*, 2002, **628**(9–10), 2067–2070.

40 R. D. Shannon, Revised effective ionic radii and systematic studies of interatomic distances in halides and chalcogenides, *Acta Crystallogr., Sect. A: Cryst. Phys., Diffr., Theor. Gen. Crystallogr.*, 1976, **32**(5), 751–767.

41 R. Shaw, D. Skovlin, B. Smith, J. Rosenthal and W. Jolly, *Lithium Bis(trimethylsilyl)amide and Tris(trimethylsilyl) amine*, 2007, pp. 19–22.

42 S. Krieck, P. Schüler, H. Görls and M. Westerhausen, Straightforward synthesis of rubidium bis (trimethylsilyl) amide and complexes of the alkali metal bis (trimethylsilyl) amides with weakly coordinating 2, 2, 5, 5-tetramethyltetrahydrofuran, *Dalton Trans.*, 2018, **47**(36), 12562–12569.

43 A. I. Ojeda-Amador, A. J. Martínez-Martínez, A. R. Kennedy and C. T. O'Hara, Structural studies of cesium, lithium/cesium, and sodium/cesium bis (trimethylsilyl) amide (HMDS) complexes, *Inorg. Chem.*, 2016, **55**(11), 5719–5728.

44 A. Dormond, A. El Bouadili, A. Aaliti and C. Moise, Insertion of carbonyl compounds into actinide—carbon σ bonds: Reactivity of [(Me3Si)2)2N]2M·Ch_2Si (Me) 2NSiMe3, *J. Organomet. Chem.*, 1985, **288**(1), C1–C5.